ACS OMEGA

Open Access

http://pubs.acs.org/journal/acsodf

Article

Ni, Co-Embedded MOF-Derived N-Doped Bimetallic Porous Carbon for Adsorption−Photocatalytic Degradation of Organic Dyes and Antibiotics

Zheng Yang,* Yi-Wu Chen, Yu-Fei Jin, Zheng Jin, Heng-Shen Xie,* Xing-Shun Cong,* and Dao-Guang Teng

Cite This: *ACS Omega* 2024, 9, 11356−11365

Read Online

ACCESS | Metrics & More | Article Recommendations | Supporting Information

ABSTRACT: An efficient protocol for photocatalytic degradation of organic dyes and antibiotics has been successfully established via MOF-derived (MOF = metal−organic framework) Ni, Co-embedded N-doped bimetallic porous carbon nanocomposites (NiCo/NC). Such a NiCo/NC nanocomposite features well-distributed structures, suitable specific surface areas, and more active sites determined by various characterization analyses. The catalyst exhibits higher photocatalytic performance and stability toward the liquid-phase degradation of methylene blue (MB) under visible light irradiation for 60 min, after the adsorption−desorption equilibrium and the thorough degradation into H_2O and CO_2. Radical quenching experiments further confirmed the dominant effect of electron holes h^+ and superoxide radical anions $\cdot O_2^-$ for the MB photodegradation process. NiCo/NC was also appropriate for the degradation of Rhodamine B, methyl orange, tetracycline hydrochloride, and norfloxacin. Moreover, NiCo/NC is robust, and its photocatalytic activity is basically maintained after 8 cycles. This work is expected to provide additional information for the design of MOF-derived carbon material with more excellent properties and lay the foundation for further industrial applications.

1. INTRODUCTION

With the rapid development of social industrialization, environmental pollution, especially water pollution, has become an urgent global problem.[1,2] The residual toxic pollutants in water, such as pesticides, antibiotics, and synthetic dyes, pose a significant threat to ecological balance and human health.[3−5] In the past few decades, many technologies have been carried out to remove dyes and antibiotics from wastewater through adsorption, advanced oxidation, biological treatments, photocatalytic degradation, and membrane technology.[6−9] Among them, adsorption is a simple and practical method. However, the single performance/low regeneration of some adsorbents and the complexity of the pollutant composition are still a problem. Hence, it is critical to develop advanced protocols combined with adsorption and catalysis, simultaneously, for effectively obviating residues of organic dyes and antibiotics in water.

Photocatalytic technology has been a promising utilization for water pollutant degradation due to its energy-saved and high efficiency, green and environmentally friendly in aqueous phase.[10] Previous studies have shown that TiO_2 semiconductors and metal oxide materials were the most common photocatalyst for the degradation of pollutants,[11−14] in which the small molecule compounds (CO_2, H_2O, and halide ions) are the primary products. However, the narrower absorption wavelengths, rapid recombination of electron−hole pairs, and the larger bandgaps result in low photocatalytic efficiency and limit practical applications.[15,16] In addition, photocorrosion originated from the photogenerated holes' accumulation is a traditional shortcoming, and the semiconductor materials are always unstable in the photocatalysis system. The corrosion of catalysts caused by light exposure in aqueous media facilitates the migration of metal ions and the dissolution of solid photocatalysts.[17,18] With the further research of photocatalysis, metal cocatalysts, such as Au, Ag, Pd, and Ni are found to tremendously advance photocatalytic performance.[19−21] The excessive use of these metals conflicts with the concept of sustainable development since their supply on Earth is limited. Nowadays, porous carbon materials are considered as a good photocatalyst for replacing metals/semiconductors because of the outstanding properties and stability.[22−24] Modified carbon matrix materials for building the functionalized catalysts could efficiently accelerate the charge transfer and dispersion.[25,26] Thus, finding stable and appropriate materials for pollutant removal with photocatalytic technology in industrialization is necessary.

Metal−organic frameworks (MOFs) are a kind of porous coordination polymer formed by metal ions/clusters and organic ligands.[27−30] Recently, carbonization of MOFs precursors has attracted great attention due to the tunable properties of the resulting materials.[31,32] In particular, MOFs have been proved to be very prospective sacrificial precursors to achieve metal or metal oxide nanoparticles embedded in porous carbon matrix with large surface areas, tunable pore

Received: September 26, 2023
Revised: December 13, 2023
Accepted: December 14, 2023
Published: February 28, 2024

sizes, good thermal stability, and homogeneously dispersed materials.[33,34] During the high-temperature pyrolysis process of MOFs, the formed carbon layers originating from the carbonization of organic ligands diffuses into the metal centers efficiently, which could accelerate the charge transfer and reduce the recombination of photogenerated charge carriers.[35,36] Therefore, these peculiar features make MOF-derived nanocomposites ideal for photocatalytic applications. For example, Cao and co-workers[37] reported the fabrication of composite materials based on nitrogen-doped carbons and CdS semiconductors derived from the Cd-MOF in situ carbonization method, as well as their application as viable photocatalysts toward tetracycline degradation under visible irradiation. Guo et al.[38] exploited excellent photodegradation efficiency of methylene blue (MB) using Co_3O_4/C nanocomposites' photocatalysts prepared from calcination of activated carbon-modified MOFs precursor. Park et al.[39] reported a ZnO-carbon composite photocatalyst with MOF-5 sheets as precursors. The catalyst showed photocatalytic RhB degradation under UV irradiation. In addition, Xia et al. explored the ZnO/N-doped nanoporous carbon materials from zeolitic imidazolate framework ZIF-8 at 800 °C.[40] The functioned composites could trap the dye molecules and enormously facilitate their photodegradation.[41] Inspired by this, the preparation of stable and high-performance porous carbon photocatalysts achieved by carbonization of self-assembled MOFs is very valuable for the degradation of organic dyes and antibiotics.

In this work, a nickel metal−organic framework (Ni-MOF) was used to fabricate Ni, Co-embedded bimetallic porous carbon nanomaterials (NiCo/NC) by a facile in situ carbonization strategy. The as-prepared NiCo/NC materials exhibited an enhanced adsorption-photocatalytic degradation of organic dyes and antibiotics. The degradation efficiencies of MB, RhB, and methyl orange (MO) reach 100%, 81.7%, and 68.4%, respectively, after the irradiation time of 60 min. In addition, the highly dispersed NiCo/NC nanoparticles demonstrated satisfactory degradation effects on tetracycline hydrochloride and norfloxacin. We further probed the reusability and regeneration of NiCo/NC 8 times. A plausible photocatalytic mechanism for MB degradation with NiCo/NC was explored via radical quenching experiments. The present study describes a new strategy of utilizing photoactive MOF-derived bimetallic porous carbon materials as an efficient catalyst for organic pollutants degradation.

2. EXPERIMENTAL SECTION

2.1. Materials. RhB, MB, MO, tetracycline hydrochloride (TCHC), and norfloxacin were provided by Energy Chemical Industrial, Inc., Shanghai, China. Ethylenediaminetetraacetic acid disodium salt (EDTA-2Na), isopropanol (IPA), 1,4-benzoquinone (BQ), $Co(NO_3)_2{\cdot}6H_2O$ (99%), 2-methylimidazole (99%), and $Ni(NO_3)_2{\cdot}6H_2O$ (98.5%) were purpased from Energy Chemical Industrial Inc., Shanghai, China, respectively. All of the solvents were obtained from commercial sources and purified by distillation prior to use.

2.2. Catalyst Preparation. ZIF-67 is synthesized via a stirring method.[42] Simply, to a 50 mL Schlenk tube under an air atmosphere were successively dissolved 2.0 g of 2-methylimidazole and 0.5 g of $Co(NO_3)_2{\cdot}6H_2O$ in 35 and 15 mL of methanol, respectively. Then, the former is quickly poured into the latter one with rapidly appearing purple precipitates. After being stirred at 60 °C for 10 h, ZIF-67 was obtained by recrystallization washing with methanol and then dried at 80 °C in vacuum for 6 h. Ni-MOF was obtained in the same way as ZIF-67, with the addition of $Ni(NO_3)_2{\cdot}6H_2O$.

Ni/ZIF-67 is prepared by the method of loading. Typically, 0.49 g of $Ni(NO_3)_2{\cdot}6H_2O$ is dissolved in 30 mL of methanol. Then, 1.0 g of ZIF-67 is dispersed in the $Ni(NO_3)_2{\cdot}6H_2O$/methanol solution followed by agitation at 40 °C for 8 h to obtain Ni/ZIF-67 by subsequent filtration, washing, and drying.

NiCo/NC was prepared by calcining and self-reducing Ni/ZIF-67. A 1.9 g portion of Ni/ZIF-67 was prepared by calcining 3 g of Ni/ZIF-67 in an Ar stream at 550 °C for 6 h. Co/NC and Ni/NC were obtained by calcining ZIF-67 and Ni-ZIF with yields of 65% and 63%, respectively.

2.3. Characterization Techniques of Materials. Powder X-ray reflection patterns (XRP) were characterized by a Bruker AXS D8 ADVANCE diffractometer with a Cu Kα source (λ = 1.5406 Å). An X-ray photoelectron spectrometer (XPS) was used for collection of the element compositions on a ESCA LAB MK-II instrument (Al Kα radiation). Microscopic images and morphologies were recorded by scanning electron microscopy (SEM) (Hitachi S-3700N) and transmission electron microscopy (TEM) (JEM-2100 200 kV) equipped with an energy dispersive X-ray spectroscopy (EDS). Specific surface areas and the pore size distributions of the materials were determined via Micromeritics 3Flex instrument at 77 K using the Brunauer−Emmett−Teller (BET) method (Autosotrb-IQ2-MP-XR).

2.4. Pollutant Adsorption and Photocatalytic Degradation. MB was used as a model pollutant to explore the adsorption-photocatalytic of precursors (ZIF-67 and Ni/ZIF-67) and NiCo/NC. The adsorption performance was evaluated by dispersing 5 mg of the material in 20 mL of MB (10 mg/L) solution with stirring in the dark at room temperature, until the adsorption and desorption equilibrium was achieved. Approximately 3 mL aliquots were sampled at a certain interval, and the solid was removed by a filter membrane (0.45 μm).

The adsorption/photodegradation of MB (%) was calculated by the following equation:

$$D(\%) = \frac{c_0 - c^*}{c_0} 100\% \quad (1)$$

where D is the percentage of degradation, C_0 is the initial concentration and C is the final concentration.

The reaction kinetic study was investigated by the pseudo first-order model equation.

$$-\ln(C/C_0) = k{\cdot}t \quad (2)$$

where k is the apparent rate constant of equation.

The photocatalytic degradation performances of materials were performed by using MB solution with a 500 W Xe lamp (λ > 420 nm). Typically, a certain amount of NiCo/NC was added into 20 mL of MB solution (10 mg/L) and then stirred for 30 min in the darkness. Then, after irradiation for an appropriate time interval, fixed amounts of the reaction system were taken out from the reactor and filtered by a 0.45 μm filter membrane for further analysis. In addition, the effects of the photocatalyst dosage (1, 3, 5, 7, and 9 mg), photocatalytic degradation time (10, 20, 30, 40, 50, and 60 min), and target pollutants (MB, RhB, MO, TC, and norfloxacin) on the photodegradation performance were thoroughly researched. And the concentration of MB, RhB, MO, TC, and norfloxacin

https://doi.org/10.1021/acsomega.3c07420
ACS Omega 2024, 9, 11356−11365

in the solutions could be determined via UV−vis spectroscopy, and the D of the target pollutants was calculated according to the eq 1.

To demonstrate the reactive species involved in the photocatalytic reaction, IPA (2 mL), EDTA-2Na (1.0 equiv), and BQ (1.0 equiv) were used in photocatalytic experiments. NiCo/NC was recycled and washed with methanol thoroughly and dried at 100 °C for 4 h. The collected sample was consecutively used for an 8-cycle experiment of MB degradation in the same condition.

3. RESULTS AND DISCUSSION

3.1. Characterization of Prepared Materials. The morphologies and structures of the synthesized Ni, Co-embedd MOF precursor, and its derived NiCo/NC were performed by scanning electron microscopy (SEM). As Figures 1a and 1b exhibited, a well-defined spherical crystal and

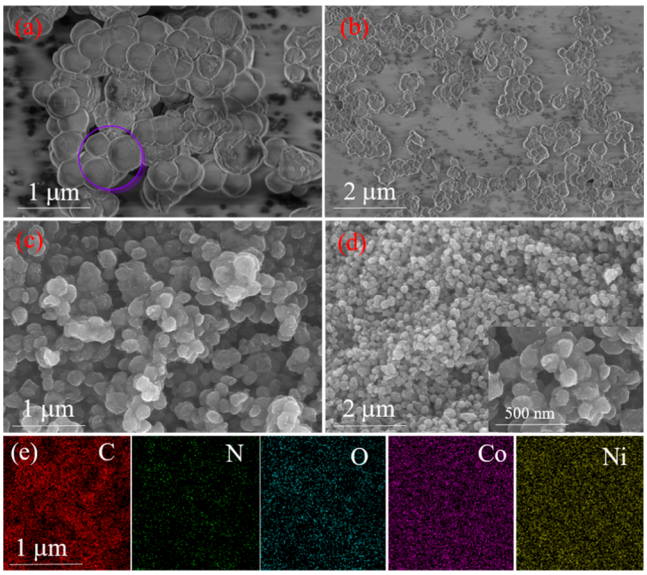

Figure 1. (a, b) SEM images of Ni/ZIF-67; (c, d) SEM images of NiCo/NC; (e) the corresponding element mapping images of C, N, O, Co, and Ni for NiCo/NC.

smooth surface of Ni/ZIF-67, approximately 1 μm in size, are clearly observed. Noteworthily, the surface of the NiCo/NC became slightly rougher with a relatively smaller particle, during the carbonization procedure of the zeolitic imidazolate framework shown in Figures 1c and 1d. Most of the metal oxide species (NiOx and/or CoOx) were reduced to Ni^0 and/or Co^0, leaving smaller porous carbon particles with a bigger pore size. Meaningfully, the porous carbon matrix materials presented a prominent property in embedding the bimetallic Ni and Co species, leading to the high dispersion characters without apparent agglomeration (Figure 1e). The homogeneous distribution of C, N, O, Co, and Ni elements on NiCo/NC surface was demonstrated by the mapping image. In addition, the contents of C, N, O, Co, and Ni are ca. 48.1, 9.89, 6.7, 17.3, and 17.6 wt %, respectively, according to the analysis with energy dispersive X-ray (EDX) (Figure S1).

The crystal structures and phase information on the prepared MOF and derived bimetallic Ni−Co/NC were examined by powder XRP as displayed in Figure 2. The XRP pattern of Ni/ZIF-67 exhibits peaks at 2θ = 14.7°, 16.4°, and 26.2°, which match well with the predicted pattern of the

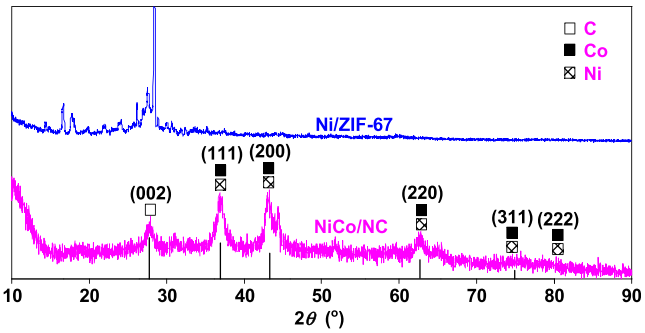

Figure 2. XRP patterns of Ni/ZIF-67 and NiCo/NC.

standard ZIF-67. A broad diffraction peak at around 26.3° observed is due to the (002) lattice plane of graphitic carbon species. Obviously, the characteristic peaks of the crystal planes from NiCo/NC at about 37.4°, 43.3°, 63.2°, 75.1°, and 80.0°, attribute to the (111), (200), (220), (311), and (222) faces of metallic NiCo and/or NiCo alloy, respectively, confirming the complete carbonization of Ni/ZIF-67.[43,44]

TEM captures the whole characteristic of the final sample. It is obvious that some uniform and favorably dispersed black nanoparticles (diameter: ∼ 20 nm) are located on the surface of NiCo/NC (Figures 3a-4c). For the high-magnification images (Figure 3d), nanosized NiCoC bimetallic nanoparticles embedded in the transparent layers of porous carbon are apparent. Figure 3e further presents a typical high-resolution TEM image for the edge of NiCo/NC, where the NiCo nanoparticles are entirely encapsulated by a carbon layer. The measured lattice spacing was 0.24 and 0.32 nm, assigning to the (111) plane of meatal NiCo and the (002) plane of graphitic carbon, respectively. The selected area electron diffraction pattern (Figure 3f) of the NiCo/NC nanoparticle verifies its polycrystalline structure.

High-resolution XPS spectra shows Ni 2p, Co 2p, C 1s, N 1s, and O 1s five elements in NiCo/NC (Figure S1). And the atomic density of C, N, O, Co, and Ni are 67.8 at. %, 12.9 at. %, 14.3 at. %, 1.3 at. %, and 3.7 at. %, respectively (Table S1), which is in accord with the EDX analysis. As shown in Figure 4a, the peaks of Ni 2p at 871.4 and 855.6 eV could be ascribed to Ni $2p_{1/2}$ and Co $2p_{3/2}$, respectively.[45] The peaks with binding energies of 870.3 eV (Ni $2p_{1/2}$) and 852.7 eV (Ni $2p_{3/2}$) are corresponding to the metallic Ni, and the peaks of Ni $2p_{1/2}$ at 871.2 and 872.8 eV and Ni $2p_{3/2}$ at 854.6, 855.0, 856.8, 859.0, and 861.4 eV could be attributed to Ni^{2+} (cobalt oxides),[46−48] while the peak at 853.3 eV confirms the existence of the carbide phase in NiCo/NC surface.[49,50] For high-resolution Co $2p_{3/2}$ spectra in Figure 4b, three characteristic peaks appeared at 778.0, 780.1, and 781.8 eV are assigned to Co^0, Co^{2+}, and Co^{3+} (cobalt oxides).[51] Obviously, some oxidation species may originate from the oxidation process on the surfaces of metal Ni and Co. In addition, among carbon regions, the sample exhibited three typical types of carbon species, contributing to the C−C (sp^2) bonds (284.5 eV), C═N/C−N (sp^2) bonds (285.8 eV), and C−O bonds (287.0 eV) (Figure 4c),[52] respectively. The N 1s curves are composed of five peaks consisting of pyridinic-N (398.6 eV), pyrrolic-N (399.4 eV), Co−N (399.5 eV), Ni−N (400.1 eV), and graphitic-N (401.6 eV),[53,54] which further proves the nitrogen was successfully doped and the presence of graphite carbon. Pyridine nitrogen and/or graphite nitrogen could increase the dispersion of NiCo surface and further improve the electron

https://doi.org/10.1021/acsomega.3c07420
ACS Omega 2024, 9, 11356−11365

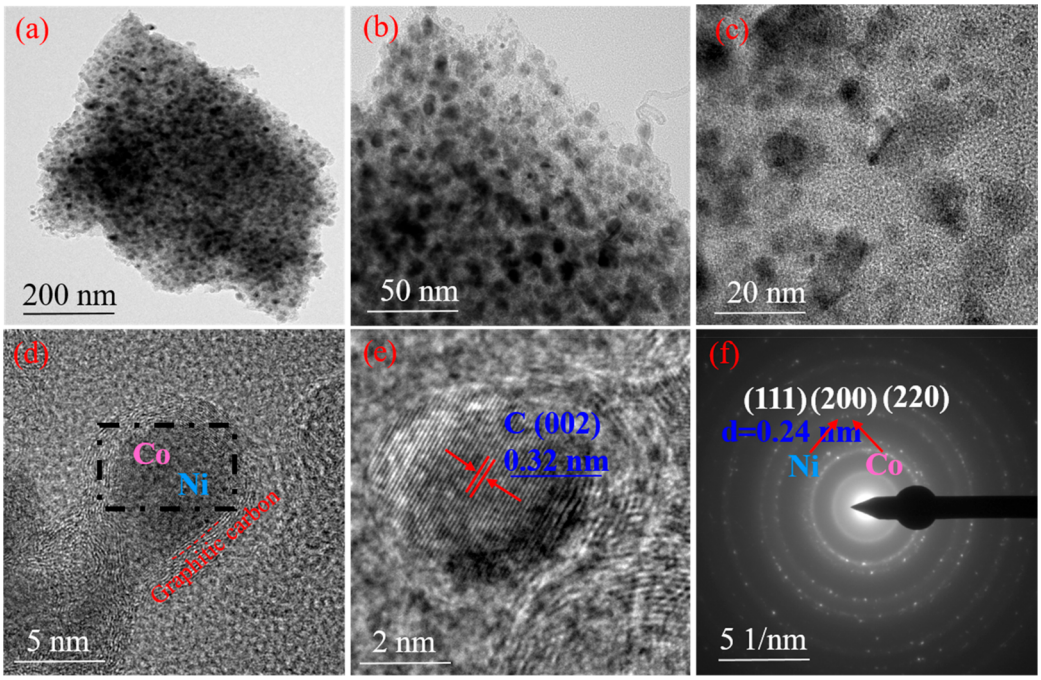

Figure 3. (a, b) TEM images, (c) enlarged TEM image, (d, e) high-magnification TEM image, and (f) electron diffraction pattern of NiCo/NC.

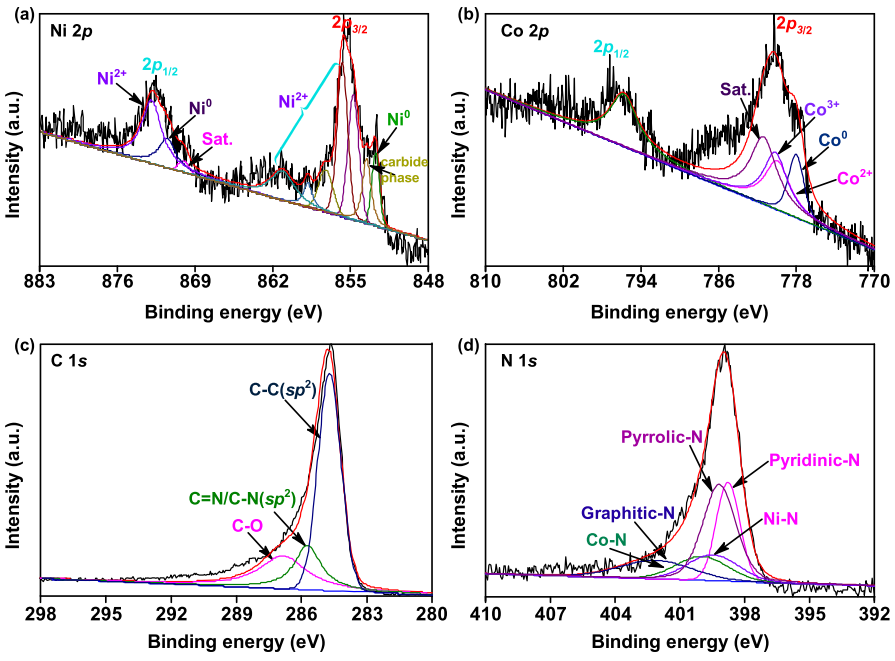

Figure 4. XPS spectra of NiCo/NC: (a) high-resolution Ni 2p spectra; (b) high-resolution Co 2p spectra; (c) high-resolution C 1s spectra; (d) high-resolution N 1s spectra.

transfer efficiency and accelerate the photochemical activities.[55,56]

As Figure 5a shows, the adsorption isotherm of NiCo/NC presents a typical type IV curve and H4 type hysteresis loop, manifesting its obvious micro/mesoporous structure (Figure 5b). In addition, the surface area of NiCo/NC was found as 413 m^2 g^{-1} with an average pore diameter of 5.7 nm (Table S2). The large micro/mesoporous characteristics of NiCo/NC are inclined to expose more active site, which could facilitate the physical transport and accelerate the adsorption-photocatalytic reaction.[57]

3.2. MB Adsorption Experiments. We performed MB adsorption experiments to better understand the adsorption capacity of NiCo/NC. Figure 6a shows the temporal UV−vis absorbance spectra of MB with NiCo/NC in darkness. The main adsorption reaction of MB occurs within the first 15 min and then gradually reaches adsorption−desorption equilibrium (Figure 6b). Only a small amount of adsorption quantity of MB increased with prolonging the time from 30 to 120 min. Moreover, compared to single adsorption or visible light irradiation, adsorption-photocatalysis presents a higher pollutant removal efficiency, which was attributed to the special

https://doi.org/10.1021/acsomega.3c07420
ACS Omega 2024, 9, 11356−11365

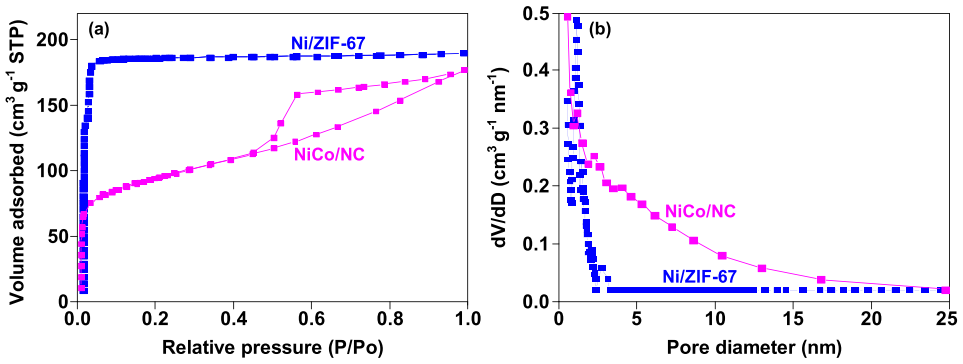

Figure 5. (a) N_2 adsorption/desorption isotherms and (b) the pore size distribution curves of Ni/ZIF-67 and NiCo/NC.

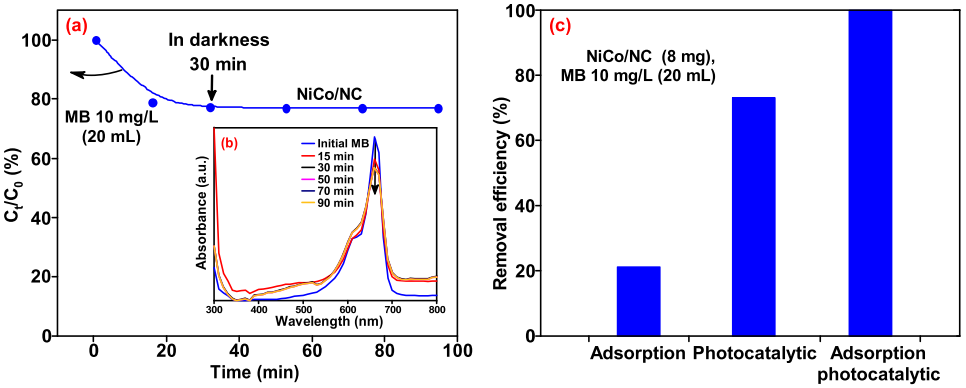

Figure 6. (a) Adsorption curves of MB on NiCo/NC in the dark. (b) Temporal UV−vis absorption spectra of MB in the presence of NiCo/NC in the dark. (c) Removal efficiency of MB over NiCo/NC under different conditions.

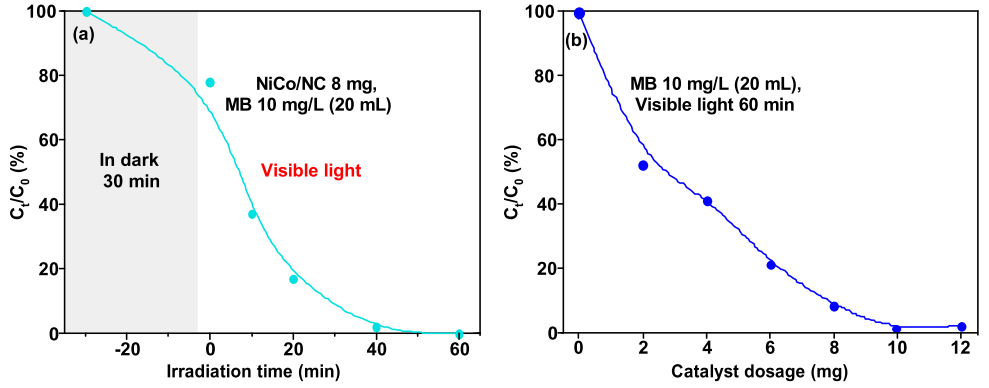

Figure 7. Total photocatalytic degradation curves of MB using NiCo/NC under light irradiation (a) contact time and (b) catalyst dosage.

composition and specific surface area and pore diameter of NiCo/NC (Figure 6c). In order to better reveal the degradation mechanism, MB was adsorbed in dark for 30 min to establish adsorption equilibrium before photocatalytic degradation by NiCo/NC.

3.3. Degradation of RhB under Different Conditions. The degradation of MB for various mass ratios of NiCo/NC and illumination time have been studied under the given conditions. As illustrated in Figure 7a, the MB decolorization efficiency is ca. 58.2% within 10 min, and it is almost entirely degraded within 60 min when 10 mg of NiCo/NC was added. Further prolonging the illumination time to 100 min has a very negligible effect on degradation efficiency. In addition, MB was not degraded within 60 min without catalyst, indicating that the self-photolysis of MB could be ignored. As shown in Figure 7b, the optimal catalyst dosage for the degradation of MB was explored in a range from 2 to 10 mg under illumination for 60 min. Approximately 60.6% MB removal efficiency could be obtained when the reaction NiCo/NC feed was lower than 4 mg, indicating the insufficient active sites were available for this adsorption−photocatalytic reaction. Interestingly, the MB removal efficiency continuously increased as the NiCo/NC amount increases from 5 to 10 mg and reaches a maximum for 8 mg. A further increase in the NiCo/NC to 12 mg does not increase the decolorization efficiency but slightly decreases, which was caused by the limitations on the charge transport and the light shielding effect for the excessive catalysts.[53]

3.4. Photocatalytic Degradation of MB with Various Materials. As listed in Figure 8a, the removal efficiency of MB was further explored over various materials for 60 min in illumination. Significantly, parent Ni/ZIF-67 presents a better adsorption capacity (in darkness 30 min) and the minimum

https://doi.org/10.1021/acsomega.3c07420
ACS Omega 2024, 9, 11356−11365

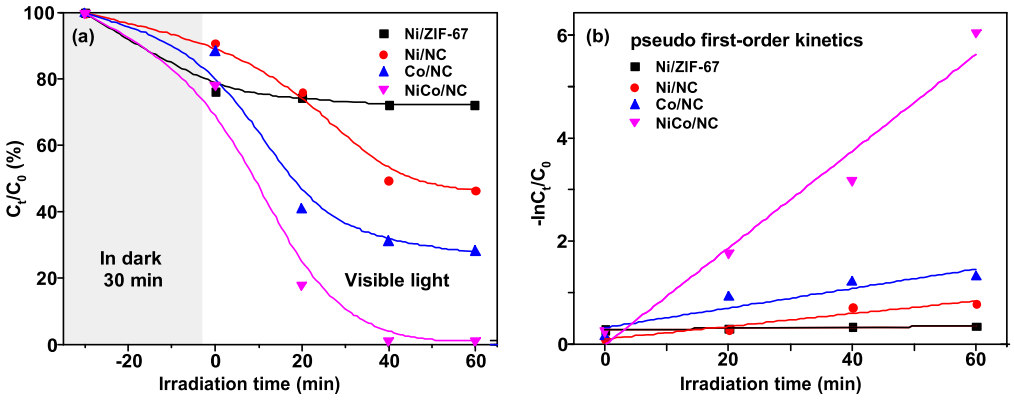

Figure 8. Photocatalytic degradation performances of MB using Ni/ZIF-67, Ni/NC, Co/NC and NiCo/NC: (a) total photocatalytic degradation curves of MB using four materials under light irradiation, (b) linear fitting of pseudo first-order kinetic equation. Reaction conditions: MB 10 mg/L (20 mL), material (8 mg), adsorption time (30 min), and photocatalytic (0−60 min).

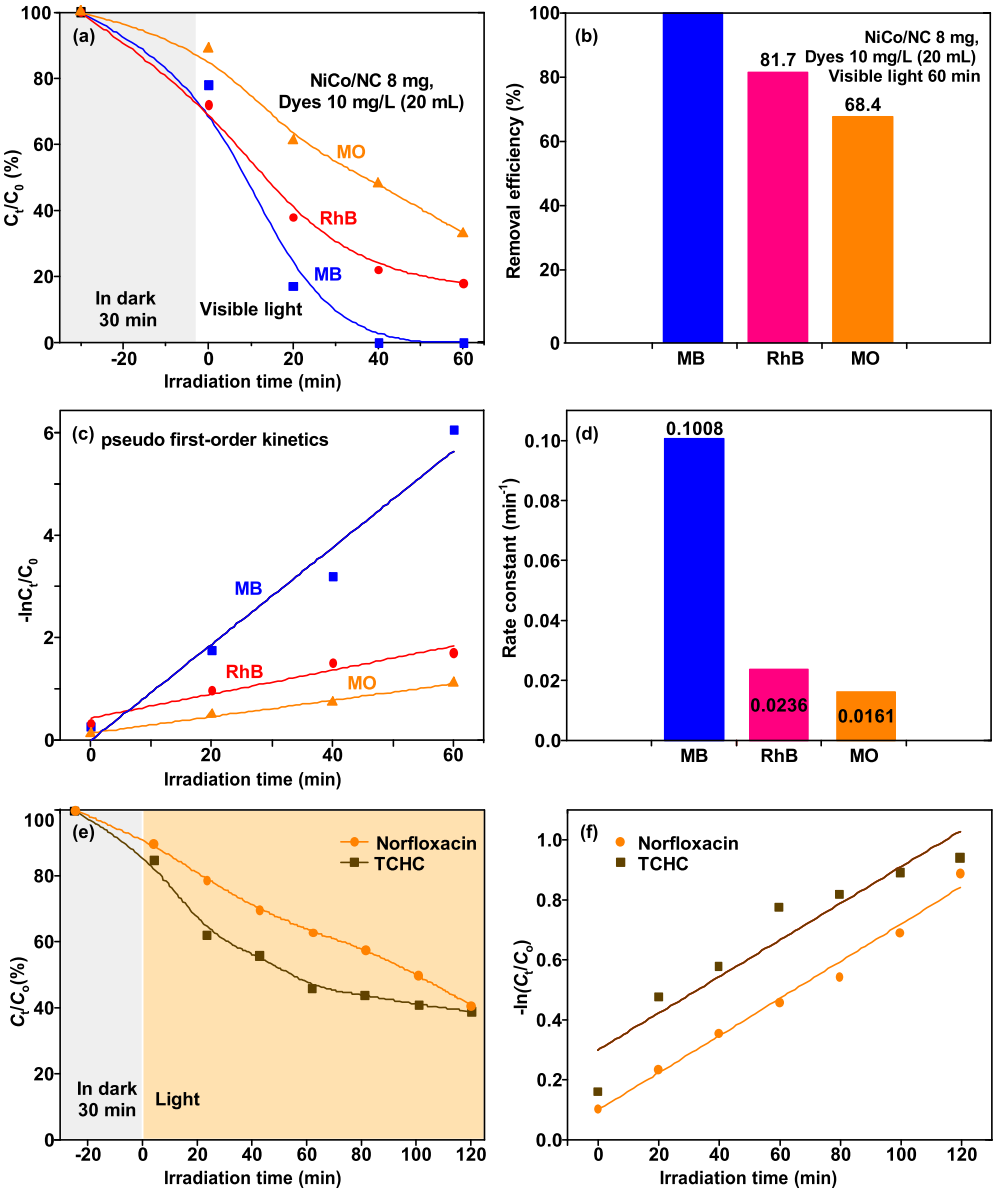

Figure 9. Photocatalytic degradation performances of NiCo/NC: (a) total photocatalytic degradation curves of MB, RhB, and MO; (b) effect of dye type on the removal efficiency under the same conditions; (c) linear fitting of pseudo first-order kinetic equation; (d) the histogram of apparent rate constant; (e) total photocatalytic degradation curves of TCHC and norfloxacin; and (f) linear fitting of pseudo first-order kinetic equation.

https://doi.org/10.1021/acsomega.3c07420
ACS Omega 2024, 9, 11356−11365

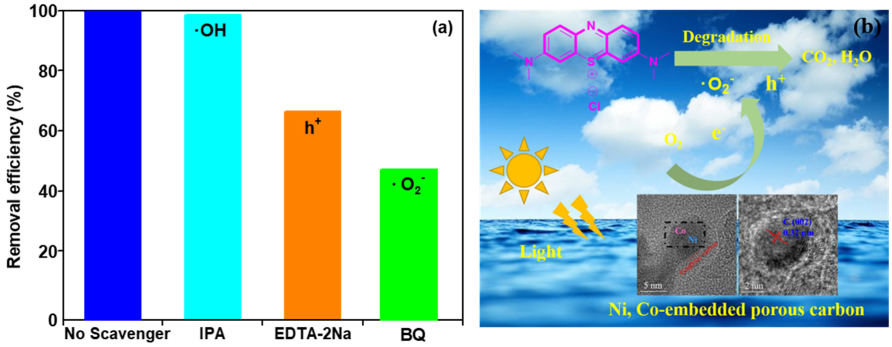

Figure 10. (a) Effect of different scavengers on the degradation of MB over NiCo/NC in water under visible light irradiation for 60 min; (b) plausible MB photocatalytic degradation mechanism with NiCo/NC under visible light irradiation.

photocatalytic removal efficiency, which could be ascribed to the higher surface area (Table S2). NiCo/NC derived from Ni/ZIF-6 exhibited excellent photocatalytic activity in this system, affording 100% MB removal efficiency. However, the poor adsorption (8.6%) and photocatalytic performance are discovered over the Ni/NC material. A crystallization aggregation effect of nickel-based catalyst could suppress the dispersion of charges and the transport of photogenerated carriers and then reduce the photocatalytic MB degradation. The Co/NC material did not obtain the desired adsorption capacity and removal efficiency. Apparently, the total removal rates of Ni/C and Co/C were only recorded as 53.6% and 72.7%, respectively. Accordingly, the removal rate of MB increased as NiCo/NC > Co/NC > Ni/NC. The results further prove that specific surface areas and adsorption abilities are a profit to MB photodegradation but not the determining factor. An sppropriate particle size could improve the surface-active catalytic sites and accelerate the photocatalytic degradation of MB.

Figure 8b exhibits the pseudo first-order kinetic model of MB photodegradation. According to the linear fitting, NiCo/NC presented the largest slope value and the steepest straight line among the four materials, indicating its excellent photocatalytic activity.[26] As expected, NiCo/NC possessed the maximum k value of 0.1008 min^{-1}, which was almost 77 times higher than that of Ni/ZIF-6 (0.00132 min^{-1}).

3.5. Photocatalytic Degradation of Other Organic Dyes and Antibiotics. To further probe the photocatalytic performance of NiCo/NC, other alternative organic dyes and antibiotics including RhB, MO, TCHC, and norfloxacin were carried out under similar conditions for the photocatalytic of MB. As shown in Figure 9a, ca. 21.8%, 27.6%, and 11.3% of the initial MB, RhB, and MO are degraded, respectively, after the adsorption process in darkness for 30 min, which demonstrated that the improvement of the photoexcited catalyst is crucial and the self-degradation is not sufficient enough. As expected, after the irradiation time of 60 min, ~99.9% of MB is removed in the presence of NiCo/NC and ca. 81.7% and 68.4% of RhB and MO, respectively, are effectively degraded (Figure 9b). It further confirms the excellent catalytic activity/photoelectric characteristic and superior light collection ability of NiCo/NC.

Figure 9c further studied the pseudo first-order kinetic model of MB, RhB, and MO photodegradation. Noteworthily, through the linear fitting, the degradation of MB displays the steepest straight line and the largest slope value among the three dyes, manifesting that the photocatalytic degradation proceeds rapidly. The maximum rate constant k value is recorded on MB (0.1008 min^{-1}), followed by RhB (0.0236 min^{-1}) and MO (0.0161 min^{-1}) (Figure 9d).

TCHC and norfloxacin are used as the targets to further evaluate the photodegradation performance of NiCo/NC. Similarly, both 14.7% of the TCHC and 10.0% of the norfloxacin are degraded with the adsorption in darkness condition for 30 min, further indicating that norfloxacin is more stable than TCHC. After 120 min irradiation, the total photocatalytic degradation efficiency of TCHC and norfloxacin are recorded to be 60.8% and 58.6%, respectively (Figure 9e).

As exhibited in Figure 9f, the reaction kinetics of TCHC and norfloxacin degradation on NiCo/NC was studied. The results comply with pseudo first-order kinetics, and their rates can be obtained from the slope of the reaction diagram. As expected, the photodegradation of TCHC reached a higher k value of 0.00995 min^{-1} in the NiCo/NC system, which was almost 3.7 times faster than that of norfloxacin (0.0027 min^{-1}). The high removal rate of organic dyes and antibiotics confirms the availability of the NiCo/NC photocatalyst.

3.6. Plausible Reaction Pathway of MB Degradation. To elucidate the mechanistic details of MB using NiCo/NC, several radical quenching experiments were performed. IPA, EDTA-2Na and BQ were used as reactive scavenger to quench hydroxyl radicals (·OH), electron holes (h^+) and superoxide radical anions ($^{\bullet}O_2^-$) species, respectively.[49] As shown in Figure 10a, MB could be nearly degraded with the addition of IPA, which further demonstrated that $^{\bullet}OH$ radical is not the main active species in the entire photocatalytic reaction mechanism. Interestingly, it was found that $^{\bullet}O_2^-$ and h^+ play a dominant role in the MB degradation process, since the removal efficiency was decreased to 64.6% and 46.3%, respectively.[50]

Based on the above experimental results and previous reports,[54] a possible pathway of the degradation mechanism of MB with NiCo/NC is described in Figure 10b. Under visible light irradiation, the electrons are excited and then transferred to the NiCo/NC surface. The photogenerated e^- could react with adsorbed O_2 on the catalyst surface to produce $^{\bullet}O_2^-$.[36] Subsequent $^{\bullet}O_2^-$ and h^+ can further oxidize MB to form small molecular product (e.g., CO_2 and H_2O).[17]

3.7. Reusability of NiCo/NC for the Photocatalytic Degradation of MB. The stability and recyclability of NiCo/NC for MB photocatalytic degradation was assessed under similar reaction conditions (8 mg of catalyst, 20 mL of MB 10 mg/L, 30 min adsorption time, 60 min photocatalytic). The catalyst was easily recycled from the reaction system because of

https://doi.org/10.1021/acsomega.3c07420
ACS Omega 2024, 9, 11356−11365

the magnetic properties (Figure S3). As exhibited in Figure 11, the NiCo/NC could be resumed 8 times without significant

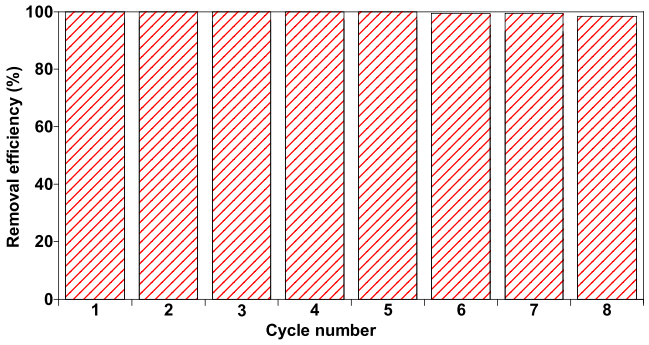

Figure 11. MB concentration changes in 8 reaction cycles with NiCo/NC (initial concentration of MB = 10 mg/L, irradiation time = 60 min).

loss of the photocatalytic performance. Over 97% of MB degradation efficiency remained in the whole circular reactions. A transmission electron microscope image of the recycled catalyst displays no severe agglomeration of the Ni, Co nanoparticles on the NiCo/NC surface, which could be attributed to the stable structure of the parent ZIF-67 MOFs (Figure S2b). These results further testified that the prepared NiCo/NC was stable and good in the field of photocatalytic applications. Furthermore, the ICP-AES analysis showed that the contents of Ni and Co were almost unchanged, indicating that Ni and/or Co species can be embedded well in the MOF-derived porous carbon layer (Table S3).

4. CONCLUSION

A novel MOF-derived N-doped bimetallic porous carbon material NiCo/NC was successfully obtained and applied to the photocatalytic degradation of organic dyes and antibiotics. The NiCo/NC catalyst with a Ni, Co-embedded carbon layer has a good photogenerated carrier capability; the available specific surface areas and well-distributed structures promote the dispersion and charges transfer, which is responsible for the adsorption−photocatalytic degradation of pollutants. Remarkably, NiCo/NC showed excellent removal efficiency for the MB within 60 min of visible light irradiation. Radical quenching experiments substantiated that h^+ and $^{\bullet}O_2^-$ dominated the photocatalytic degradation process of MB. Furthermore, NiCo/NC is highly active for the degradation of other organic dyes and antibiotics, such as RhB, MO, TCHC and norfloxacin. Simultaneously, NiCo/NC is stable, and its photocatalytic performance is adequately maintained after 8 reaction cycles. This work would provide a flexible protocol for fabrication of the recyclable embedded metal carbon materials for degradation of pollutants.

■ ASSOCIATED CONTENT

Supporting Information

The Supporting Information is available free of charge at https://pubs.acs.org/doi/10.1021/acsomega.3c07420.

Physical and chemical nature of materials (Ni/ZIF-67 and NiCo/NC) (Figures S1, S2 and S3; Tables S1 and S2), and pore texture parameters of NiCo/NC (Table S3) (PDF)

■ AUTHOR INFORMATION

Corresponding Authors

Zheng Yang − *School of Architectural Intelligence, Jiangsu Vocational Institute of Architectural Technology, Xuzhou 221116, P. R. China; Jiangsu Collaborative Innovation Center for Building Energy Saving and Construct Technology, Xuzhou 221116, P. R. China; Jiangsu Engineering Laboratory of Biomass Resources Comprehensive Utilization, Jiangsu Vocational Institute of Architectural Technology, Xuzhou 221116, P. R. China; College of Chemical Engineering, Zaozhuang University, Zaozhuang 277160, P. R. China;* orcid.org/0000-0001-6504-9145; Email: hkxie_xz@163.com

Heng-Shen Xie − *Jiangsu Engineering Laboratory of Biomass Resources Comprehensive Utilization, Jiangsu Vocational Institute of Architectural Technology, Xuzhou 221116, P. R. China*; Email: cong_xingshun@126.com

Xing-Shun Cong − *College of Chemical Engineering, Zaozhuang University, Zaozhuang 277160, P. R. China;* orcid.org/0000-0003-1825-9486; Email: yang_chem@126.com

Authors

Yi-Wu Chen − *School of Architectural Intelligence, Jiangsu Vocational Institute of Architectural Technology, Xuzhou 221116, P. R. China*

Yu-Fei Jin − *School of Architectural Intelligence, Jiangsu Vocational Institute of Architectural Technology, Xuzhou 221116, P. R. China*

Zheng Jin − *School of Architectural Intelligence, Jiangsu Vocational Institute of Architectural Technology, Xuzhou 221116, P. R. China*

Dao-Guang Teng − *School of Chemical Engineering, Zhengzhou University, Zhengzhou 450001, P. R. China;* orcid.org/0000-0001-9120-3070

Complete contact information is available at: https://pubs.acs.org/10.1021/acsomega.3c07420

Notes

The authors declare no competing financial interest.

■ ACKNOWLEDGMENTS

This work was financially supported by the Natural Science Foundation of the Jiangsu Higher Education Institution of China (Grant 20KJB530014), the Doctor Special Research Funds of Jiangsu Collaborative Innovation Center for Building Energy Saving and Construct Technology (SJXTBS2120 and SJXTBS2103), the Higher Education Reform Research Project of Jiangsu Province (Grant 2021JSJG467), the Natural Science Foundation of Shandong Province (Grants ZR2022MB027 and ZR2022QB093), and the National Natural Science Foundation of China (Grant 51674223).

■ REFERENCES

(1) Rochkind, M.; Pasternak, S.; Paz, Y. Using Dyes for evaluating photocatalytic properties: A critical review. *Molecules* **2015**, *20*, 88−110.

(2) Lim, S.; Shi, J. L.; von Gunten, U.; McCurry, D. L. Ozonation of organic compounds in water and wastewater: A critical review. *Water Res.* **2022**, *213*, 118053.

(3) Auerbach, E. A.; Seyfried, E. E.; McMahon, K. D. Tetracycline resistance genes in activated sludge wastewater treatment plants. *Water Res.* **2007**, *41*, 1143−1151.

(4) Mashkoor, F.; Nasar, A. Magsorbents: potential candidates in wastewater treatment technology e a review on the removal of methylene blue dye. *J. Magn. Magn Mater.* **2020**, *500*, 166408−166426.
(5) Al-Buriahi, A. K.; Al-Gheethi, A. A.; Senthil Kumar, P.; Radin Mohamed, R. M. S.; Yusof, H.; Alshalif, A. F.; Khalifa, N. A. Elimination of rhodamine B from textile wastewater using nanoparticle photocatalysts: A review for sustainable approaches. *Chemosphere* **2022**, *287*, 132162.
(6) Katheresan, V.; Kansedo, J.; Lau, S. Y. Efficiency of various recent wastewater dye removal methods: A review. *J. Environ. Chem. Eng.* **2018**, *6*, 4676−4697.
(7) He, H. B.; Luo, Z. Z.; Tang, Z. Y.; Yu, C. L. Controllable construction of $ZnWO_4$ nanostructure with enhanced performance for photosensitized Cr (VI) reduction. *Appl. Surf. Sci.* **2019**, *490*, 460−468.
(8) Oar-Arteta, L.; Wezendonk, T.; Sun, X.; Kapteijn, F.; Gascon, J. Metal organic frameworks as precursors for the manufacture of advanced catalytic materials. *Mater. Chem. Front.* **2017**, *1*, 1709−1745.
(9) Kong, Z.; Li, L.; Xue, Y.; Yang, M.; Li, Y.Y. Challenges and prospects for the anaerobic treatment of chemical-industrial organic wastewater: A review. *J. Clean. Prod.* **2019**, *231*, 913−927.
(10) Zhang, S.; Li, B.; Wang, X.; Zhao, G.; Hu, B.; Lu, Z.; Wen, T.; Chen, J.; Wang, X. Recent developments of two-dimensional graphene-based composites in visible-light photocatalysis for eliminating persistent organic pollutants from wastewater. *Chem. Eng. J.* **2020**, *390*, 124642.
(11) Kim, J. R.; Kan, E. Heterogeneous photocatalytic degradation of sulfamethoxazole in water using a biochar-supported TiO_2 photocatalyst. *J. Environ. Manag.* **2016**, *180*, 94−101.
(12) Kar, A.; Sain, S.; Rossouw, D.; Knappett, B. R.; Pradhan, S. K.; Wheatley, A. E. H. Facile synthesis of SnO_2-PbS nanocomposites with controlled structure for applications in photocatalysis. *Nanoscale* **2016**, *8*, 2727−2739.
(13) Guo, Q.; Zhou, C.Y.; Ma, Z.B.; Yang, X.M. Fundamentals of TiO_2 photocatalysis: concepts, mechanisms, and challenges. *Adv. Mater.* **2019**, *31*, 1901997.
(14) Wen, W.; Hai, J. H.; Yao, J. C.; Gu, Y. J.; Kobayashi, H.; Tian, H.; Sun, T. L.; Chen, Q. Y.; Yang, P.; Geng, C.; Wu, J. M. Univariate lattice parameter modulation of single-crystal-like anatase TiO_2 hierarchical nanowire arrays to improve photoactivity. *Chem. Mater.* **2021**, *33*, 1489−1497.
(15) Di Liberto, G.; Tosoni, S.; Pacchioni, G. Role of heterojunction in charge carrier separation in coexposed anatase (001)-(101) surfaces. *J. Phys. Chem. Lett.* **2019**, *10*, 2372−2377.
(16) Livraghi, S.; Paganini, M. C.; Giamello, E.; Selloni, A.; Di Valentin, C.; Pacchioni, G. Origin of photoactivity of nitrogen-doped titanium dioxide under visible light. *J. Am. Chem. Soc.* **2006**, *128*, 15666−15671.
(17) Sha, Z.; Chan, H. S.; Wu, J. Ag_2CO_3/UiO-66(Zr) composite with enhanced visible-light promoted photocatalytic activity for dye degradation. *J. Hazard. Mater.* **2015**, *299*, 132−140.
(18) Xiang, X.; Zhu, B.; Cheng, B.; Yu, J.; Lv, H. Enhanced photocatalytic H_2-production activity of CdS quantum dots using Sn^{2+} as cocatalyst under visible light irradiation. *Small* **2020**, *16*, 2001024.
(19) Shi, R.; Cao, Y.; Bao, Y.; Zhao, Y.; Waterhouse, G. I. N.; Fang, Z.; Wu, L. Z.; Tung, C. H.; Yin, Y.; Zhang, T. Self-assembled Au/CdSe nanocrystal clusters for plasmon-mediated photocatalytic hydrogen evolution. *Adv. Mater.* **2017**, *29*, 1700803.
(20) Fei, J.; Li, J. Controlled preparation of porous TiO_2-Ag nanostructures through supramolecular assembly for plasmon-enhanced photocatalysis. *Adv. Mater.* **2015**, *27*, 314.
(21) Xiao, N.; Li, S.; Liu, S.; Xu, B.; Li, Y.; Gao, Y.; Ge, L.; Lu, G. Novel PtPd alloy nanoparticle-decorated g-C_3N_4 nanosheets with enhanced photocatalytic activity for H_2 evolution under visible light irradiation. *Chin. J. Catal.* **2019**, *40*, 352−361.
(22) Sun, X.; Habibul, N.; Du, H. Co0.85Se magnetic nanoparticles supported on carbon nanotubes as catalyst for hydrogen evolution reaction. *Chin. J. Catal.* **2021**, *42*, 235−243.
(23) Tsao, C.-W.; Fang, M.-J.; Hsu, Y.-J. Modulation of interfacial charge dynamics of semiconductor heterostructures for advanced photocatalytic applications. *Coordin. Chem. Rev.* **2021**, *438*, 213876.
(24) Feng, X.; Li, X.; Luo, H.; Su, B.; Ma, J. Facile synthesis of Ni-based layered double hydroxides with superior photocatalytic performance for tetracycline antibiotic degradation. *J. Solid. State Chem.* **2022**, *307*, 122827.
(25) Yang, S. J.; Nam, S.; Kim, T.; Im, J. H.; Jung, H.; Kang, J. H.; Wi, S.; Park, B.; Park, C. R. Preparation and exceptional lithium anodic performance of porous carbon-coated ZnO quantum dots derived from a metal-organic framework. *J. Am. Chem. Soc.* **2013**, *135*, 7394−7397.
(26) Bie, C. B.; Yu, H. G.; Cheng, B.; Ho, W.; Fan, J. J.; Yu, J. G. Design, fabrication, and mechanism of nitrogen-doped graphene-based photocatalyst. *Adv. Mater.* **2021**, *33*, 2003521.
(27) Yaghi, O. M.; O'Keeffe, M.; Ockwig, N. W.; Chae, H. K.; Eddaoudi, M.; Kim, J. Reticular synthesis and the design of new materials. *Nature* **2003**, *423*, 705−714.
(28) Banerjee, R.; Furukawa, H.; Britt, D.; Knobler, C.; O'Keeffe, M.; Yaghi, O. M. Control of pore size and functionality in isoreticular zeolitic imidazolate frameworks and their carbon dioxide selective capture properties. *J. Am. Chem. Soc.* **2009**, *131*, 3875−3877.
(29) Hu, P.; Morabito, J. V.; Tsung, C. K. Core-shell catalysts of metal nanoparticle core and metal-organic framework shell. *ACS Catal.* **2014**, *4*, 4409−4419.
(30) Xiao, J. D.; Jiang, H. L. Metal-organic frameworks for photocatalysis and photothermal catalysis. *Acc. Chem. Res.* **2019**, *52*, 356−366.
(31) Zheng, F. C.; Yang, Y.; Chen, Q. W. High lithium anodic performance of highly nitrogen-doped porous carbon prepared from a metal-organic framework. *Nat. Commun.* **2014**, *5*, 5261.
(32) Salunkhe, R. R.; Kaneti, Y. V.; Kim, J.; Kim, J. H.; Yamauchi, Y. Nanoarchitectures for metal-organic framework-derived nanoporous carbons toward supercapacitor applications. *Acc. Chem. Res.* **2016**, *49*, 2796−2806.
(33) Zhong, W.; Liu, H.; Bai, C.; Liao, S.; Li, Y. Base-free oxidation of alcohols to esters at room temperature and atmospheric conditions using nanoscale Co-based catalysts. *ACS Catal.* **2015**, *5*, 1850−1856.
(34) Li, J.; Xia, W.; Tang, J.; Tan, H.; Wang, J.; Kaneti, Y.; Bando, Y.; Wang, T.; He, J.; Yamauchi, Y. MOF nanoleaves as new sacrificial templates for the fabrication of nanoporous Co-Nx/C electrocatalysts for oxygen reduction. *Nanoscale Horiz.* **2019**, *4*, 1006−1013.
(35) Jiang, H. L.; Liu, B.; Lan, Y. Q.; Kuratani, K.; Akita, T.; Shioyama, H.; Zong, F. Q.; Xu, Q. From metal-organic framework to nanoporous carbon: toward a very high surface area and hydrogen uptake. *J. Am. Chem. Soc.* **2011**, *133*, 11854−11857.
(36) Yang, Z.; Xie, H. S.; Lin, W. Y.; Chen, Y. W.; Teng, D.; Cong, X. S. Enhanced adsorption-photocatalytic degradation of organic pollutants *via* a ZIF-67-derived Co-N codoped carbon matrix catalyst. *ACS Omega* **2022**, *7*, 40882−40891.
(37) Cao, H. L.; Cai, F. Y.; Yu, K.; Zhang, Y. Q.; Lü, J.; Cao, R. Photocatalytic degradation of tetracycline antibiotics over CdS/nitrogen-doped-carbon composites derived from in situ carbonization of metal-organic frameworks. *ACS Sustainable Chem. Eng.* **2019**, *7*, 10847−10854.
(38) Guo, J.; Zhang, Y.; He, Y. C.; Shan, J. Photocatalytic performance of Co_3O_4/C based on ZIF-67/C composite materials. *Polyhedron* **2020**, *175*, 114215.
(39) Yang, S. J.; Im, J. H.; Kim, T.; Lee, K.; Park, C. R. MOF-derived ZnO and ZnO@C composites with high photocatalytic activity and adsorption capacity. *J. Hazard. Mater.* **2011**, *186*, 376−382.
(40) Chen, B.; Ma, G.; Kong, D.; Zhu, Y.; Xia, Y. Atomically homogeneous dispersed ZnO/N-doped nanoporous carbon composites with enhanced CO_2 uptake capacities and high efficient organic pollutants removal from water. *Carbon* **2015**, *95*, 113−124.

https://doi.org/10.1021/acsomega.3c07420
ACS Omega 2024, 9, 11356−11365

(41) Hussain, M. Z.; Schneemann, A.; Fischer, R. A.; Zhu, Y.; Xia, Y. MOF derived porous ZnO/C nanocomposites for efficient dye photodegradation. *ACS Appl. Energy Mater.* **2018**, *1*, 4695−4707.
(42) Qian, J.; Sun, F.; Qin, L. Hydrothermal synthesis of zeolitic imidazolate framework-67 (ZIF-67) nanocrystals. *Mater. Lett.* **2012**, *82*, 220−223.
(43) Das, R.; Pachfule, P.; Banerjee, R.; Poddar, P. Metal and metal oxide nanoparticle synthesis from metal organic frameworks (MOFs): finding the border of metal and metal oxides. *Nano.* **2012**, *4*, 591−599.
(44) Zhang, F.; Yuan, C.; Zhu, J.; Wang, J.; Zhang, X.; Lou, X. Flexible films derived from electrospun carbon nanofibers incorporated with Co_3O_4 hollow nanoparticles as self-supported electrodes for electrochemical capacitors. *Adv. Funct. Mater.* **2013**, *23*, 3909−3915.
(45) Barreca, D.; Massignan, C.; Daolio, S.; Fabrizio, M.; Piccirillo, C.; Armelao, L.; Tondello, E. Composition and microstructure of cobalt oxide thin films obtained from a novel cobalt(II) precursor by chemical vapor deposition. *Chem. Mater.* **2001**, *13*, 588−593.
(46) Goto, Y.; Taniguchi, K.; Omata, T.; Otsuka-Yao-Matsuo, S.; Ohashi, N.; Ueda, S.; Yoshikawa, H.; Yamashita, Y.; Oohashi, H.; Kobayashi, A. K. Formation of Ni_3C nanocrystals by thermolysis of nickel acetylacetonate in oleylamine: characterization using hard X-ray photoelectron spectroscopy. *Chem. Mater.* **2008**, *20*, 4156−4160.
(47) Pang, F.; Song, F.; Zhang, Q.; Tan, Y.; Han, Y. Study on the influence of oxygencontaining groups on the performance of Ni/AC catalysts in methanol vaporphase carbonylation. *Chem. Eng. J.* **2016**, *293*, 129−138.
(48) Guo, H. J.; Zhang, H. R.; Zhang, L. Q.; Wang, C.; Peng, F.; Huang, Q. L.; Xiong, L.; Huang, C.; Ouyang, X. P.; Chen, X. D.; Qiu, X. Q. Selective hydrogenation of furfural to furfuryl alcohol over acid-activated attapulgite-supported NiCoB amorphous alloy catalyst. *Ind. Eng. Chem. Res.* **2018**, *57*, 498−511.
(49) Fan, X.; Peng, Z.; Ye, R.; Zhou, H.; Guo, X. M_3C (M: Fe, Co, Ni) nanocrystals encased in graphene nanoribbons: an active and stable bifunctional electrocatalyst for oxygen reduction and hydrogen evolution reactions. *ACS Nano* **2015**, *9*, 7407−7418.
(50) Su, Y. P.; Chen, C.; Zhu, X. G.; Zhang, Y.; Gong, W. B.; Zhang, H. M.; Zhao, H. J.; Wang, G. Z. Carbon-embedded Ni nanocatalysts derived from MOFs by a sacrificial template method for efficient hydrogenation of furfural to tetrahydrofurfuryl alcohol. *Dalton Trans.* **2017**, *46*, 6358−6365.
(51) Collinge, G.; Xiang, Y. Z.; Barbosa, R.; McEwen, J. S.; Kruse, N. CO-induced inversion of the layer sequence of a model CoCu catalyst. *Surf. Sci.* **2016**, *648*, 74−83.
(52) Wang, Z.; Peng, S.; Hu, Y.; Li, L.; Yan, T.; Yang, G.; Ji, D.; Srinivasan, M.; Pan, Z.; Ramakrishna, S. Cobalt nanoparticles encapsulated in carbon nanotube-grafted nitrogen and sulfur Co-doped multichannel carbon fibers as efficient bifunctional oxygen electrocatalysts. *J. Mater. Chem. A* **2017**, *5*, 4949−4961.
(53) Xue, Y.; Liu, J.; Chen, H.; Wang, R.; Li, D.; Qu, J.; Dai, L. Nitrogen-doped graphene foams as metal-free counter electrodes in high-performance dye-sensitized solar cells. *Angew. Chem., Int. Ed.* **2012**, *51*, 12124−12127.
(54) Chen, L.; Xu, C.; Du, R.; Mao, Y.; Xue, C.; Chen, L.; Qu, L.; Zhang, J.; Yi, T. Rational design of three-dimensional nitrogen-doped carbon nanoleaf networks for high performance oxygen reduction. *J. Mater. Chem. A* **2015**, *3*, 5617−5627.
(55) Wang, S.; Guan, B. Y.; Lou, X. W. Rationally designed hierarchical N-doped carbon@$NiCo_2O_4$ double-shelled nanoboxes for enhanced visible light CO_2 reduction. *Energy Environ. Sci.* **2018**, *11*, 306−310.
(56) Xie, X.; Su, D.; Zhang, J.; Chen, S.; Mondal, A. K.; Wang, G. A comparative investigation on the effects of nitrogen-doping into graphene on enhancing the electrochemical performance of SnO_2/graphene for sodium-ion batteries. *Nanoscale* **2015**, *7*, 3164−3172.
(57) Ouyang, T.; Cheng, K.; Gao, Y.; Kong, S.; Ye, K.; Wang, G.; Cao, D. Molten salt synthesis of nitrogen doped porous carbon: A new preparation methodology for highvolumetric capacitance electrode materials. *J. Mater. Chem. A* **2016**, *4*, 9832−9843.

https://doi.org/10.1021/acsomega.3c07420
ACS Omega 2024, 9, 11356−11365